Characterizations of Mutual Coupling Effects on Switch-Based Phased Array Antennas for 5G Millimeter-Wave Mobile Communications

N.B. When citing this work, cite the original published paper.

(article starts on next page)

Characterizations of Mutual Coupling Effects on Switch-Based Phased Array Antennas for 5G Millimeter-Wave Mobile Communications

XIAOMING CHEN[ID][1], **(Member, IEEE), MUHAMMAD ABDULLAH**[1], **QINLONG LI**[1],
JIANXING LI[ID][1], **(Member, IEEE), ANXUE ZHANG**[1], **AND**
TOMMY SVENSSON[ID][2], **(Senior Member, IEEE)**

[1] School of Electronic and Information Engineering, Xi'an Jiaotong University, Xi'an 710049, China
[2] Department of Electrical Engineering, Chalmers University of Technology, 41296 Gothenburg, Sweden

Corresponding author: Xiaoming Chen (xiaoming.chen@mail.xjtu.edu.cn)

ABSTRACT The fifth generation (5G) millimeter-wave (mmWave) handset demands a cost-effective mmWave array antenna with beam steering capability to overcome the high-pass loss and to ensure seamless connectivity. Unlike sub-6-GHz handsets, emerging mmWave handsets usually employ phased array antennas with a reasonably large number of elements. Unfortunately, due to the legacy of a few antennas in sub-6-GHz handsets, the mutual coupling effect on the mmWave handset has not been thoroughly investigated. In this paper, we study the mutual coupling effect on the mmWave handset performance by comparing array antennas with different inter-element spacing and different configurations. It is found that mutual coupling tends to increase the active reflection (especially at large scanning angles), which in turn reduces the realized gain and maximum scanning angle of the phased array antenna. For a sub-6-GHz multiple-input multiple-output handset with two or four antenna ports and fully digital precoding/decoding, 10-dB isolation is usually regarded as good enough. It is shown in this paper, however, that the outage capacity of the mmWave handset can be clearly improved by reducing the mutual coupling.

INDEX TERMS Active reflection, handset array, millimeter-wave (mmWave), multiple-input multiple-output (MIMO), mutual coupling.

I. INTRODUCTION

The ever growing data rate explosion in mobile communications has drawn considerable attention to the millimeter-wave (mmWave) frequency bands, where huge spectrum is available to fulfill the high traffic demand of the fifth generation (5G) communications [1]–[4]. However, there are quite a few challenges for mmWave mobile communications (as compared with the legacy sub-6 GHz cellular communications). For examples, the path losses in the mmWave frequency bands are considerably higher and it is tougher to track mobile users. Thus, (efficient) adaptive beamforming is usually required at both transmitter and receiver to overcome the high path loss and to ensure seamless connectivity.

In addition, mmWave circuits are expensive, lossy, and power hungry, as compared with the conventional radio frequency (RF) circuits. To solve these issues, hybrid beamforming is proposed [5]. By combining digital beamforming with analogue beamforming, hybrid beamforming can saves the system cost significantly by using fewer RF chains while still having comparable performance as compared with the fully digital beamforming. A challenge of the hybrid beamforming system is the high computational complexity. Sophisticated algorithms are needed, e.g., to estimate the channel [5]. Such high computational complexity is affordable at the base station, but is not suitable for battery-driven mobile devices. Therefore, phased array antennas were first proposed for 5G mmWave handsets in [6], where it is assumed that each array element has broad beam (i.e., fan beam [6]) e.g., in the elevation plane and the array can perform beam steering in

the azimuth plane. Two of such arrays at either two short edges [6] or two long edges [7] of the handset are needed to cover the whole sphere.

Beam switching networks based on Rotman lens [8] or Butler matrix [9] were proposed for mmWave mobile applications. These schemes require a switch to enable beam switching. A drawback of these schemes is that the beam switching network is so bulky that only one linear array can be supported on a normal mobile phone chassis. Therefore, it is difficult to cover the whole sphere using these schemes. In practice, the antenna ports are directly connected to mmWave chips, where the analogue beamforming is executed. As a result, the focus for 28-GHz (or lower frequencies) mmWave handsets is mainly on antenna design. The antenna ports are then connected to chips via coaxial cables. (The commercially available cable in this frequency band is about 0.51 mm in diameter.) It is noted that due to the increased insertion loss of mmWave cables, array antennas at 60 GHz or higher frequencies are usually integrated on mmWave chips. Nevertheless, the implementation for 60-GHz mmWave handsets is much more challenging due to the severe hardware impairments (e.g., large oscillator phase noise) and high penetration loss from the handset case [10]. Therefore, it is foreseen that mmWave handsets will firstly be available at 28 GHz or lower frequencies [11]. As a result, we focus on 28-GHz mmWave array antennas in this work.

To ensure seamless connection of 5G mmWave communications with affordable cost at the mobile terminal side, switch-based phased array antennas were proposed in [12] and [13]. In order to cover the full sphere, the total array is composed of three subarrays, each roughly covers a broad sector in phi (theta) plane and can perform RF beam steering in theta (phi) plane. The three subarrays are connected via a switch. A great deal of effort has been exerted on improving antenna characteristics (such as return losses) and on investigating the user effects on the radiation characteristics [7], [12]–[15] and spherical coverage [16]. However, almost all of the mmWave handset works simply present isolation values without careful investigation of the mutual coupling effect for 5G mmWave communications. Although the mutual coupling effect on conventional arrays and multiple-input multiple-output (MIMO) systems have been studied extensively in the literature (see [17], [18] and references therein), its study in the context of 5G mmWave handset is limited. This is probably due to the common belief that the mutual coupling effect on the handset is far less than that on the base station where large arrays are usually employed. This can be true for the conventional sub-6 GHz cellular system, where the mobile handset typically has two or four antennas (each connected with the MIMO transceiver via a complete RF chain, i.e., fully digital precoding/decoding). However, the mutual coupling effect becomes more severe as the number of antennas increases and due to the fact that many antenna elements are needed at mmWave handset (which has distinct transceiver architecture as compared with its sub-6 GHz counterpart), mutual coupling as low as −15 dB can still have non-negligible influence on the performance of the mmWave handset. Thus, the mutual coupling in the mmWave handset deserves more investigation.

In this work, we examine the mutual coupling effect using examples of the switch-based phased array antennas for 5G mmWave handsets. We show that the mutual coupling degrades the active reflections within each subarray. The latter not only causes a reduction of the realized gain (and, therefore, the received power in the downlink) of each subarray, but also limits the scanning range of each subarray (which, in turn, increases the outage probability of the mmWave communications.) To ensure the overall performance of the mmWave handset, the mutual coupling must be mitigated.

Many mutual coupling reduction techniques exist in the literature, yet most of them are not suitable for the mmWave handset. For example, the complexity of the decoupling network [19] increases drastically as the number of antenna elements increases and becomes prohibitive for mmWave array antennas; metasurface based techniques [20], [21] usually dictate high profile array antennas, which are less suitable for mmWave handsets; the characteristic mode technique [22] is not suitable for mmWave handsets either, because there are mainly travelling waves propagating along the chassis at mmWave frequencies. The array-antenna decoupling surface (ADS) technique [23] offers a promising solution for large arrays. However, the ADS needs to be at least quarter-wavelength (2.7 mm at 28 GHz) away from the array, which inevitably increases the profile of the handset. As a result, we study the mutual coupling effect on mmWave handsets by varying the inter-element spacing and by comparing array antennas with the same inter-element spacing yet different configurations. We show that, by judicious design of the array elements, the mutual coupling can be reduced and the scanning range can be increased. It is shown that, by reducing the mutual coupling, the outage capacity [24] (simulated using a realistic mmWave channel model) can be substantially improved.

II. MUTUAL COUPLING EFFECTS ON BEAM STEERING

As mentioned in the introduction, we use the switch-based phased array [13] as an example to study the mutual coupling effect. Specifically, we use the square patch antenna as the array element. The handset array is shown in Fig. 1. As can be seen, the whole array is composed of three subarrays and each subarray consists of eight patch elements. When establishing communications in the downlink, we first sweep over the three subarrays and choose the one that receives the highest power, then perform RF beamforming using the selected subarray. As found out in the simulation results later, by using the bisection method (cf. Section IV) in searching for the strongest scanning angle, it takes just a few searches for the RF beamforming to converge. Thus, the initial access at the user side can be established very fast using the switch-based phased array.

Since the three subarrays are identical and they are selected sequentially via a single-pole-triple-throw switch, and the
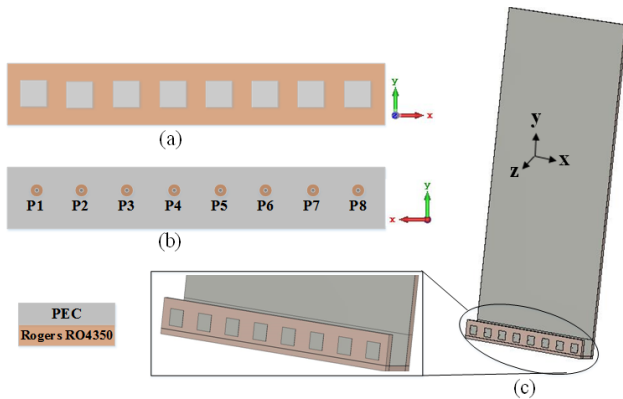
FIGURE 1. CST model of the switch-based phased array: (a) front side of a subarray; (b) back side of a subarray; (c) the whole array composed of three subarrays together with chassis. The broadsides of the three subarrays are facing toward +z, −z, and −y directions, respectively. P1-P8 represents ports 1-8 of one subarray.

mutual coupling between subarrays is very low, it suffices to investigate the mutual coupling effect on one subarray in this section. For the same reasons, in the next section we investigate mutual coupling reduction schemes on the subarray. (Note that the correlation coefficients for MIMO antennas do not apply to phased array in that there is only one antenna port per phased array.)

We first use a square patch element with a dimension of 2.46 mm (0.22λ, where λ represents the free-space wavelength at 28 GHz). The substrate is Rogers R04350B with a relative permittivity of 3.48, a loss tangent of 0.0037, and a height of 0.8 mm. To study the mutual coupling effect, we first use one subarray (i.e., a uniform linear array) with varying inter-element spacing of $\lambda/2$, $\lambda/3$, and $\lambda/4$. CST microwave studio is used for simulations in this work. During the simulations, we use 15 cells per wavelength and open boundaries for all the six surfaces.

The obtained scattering parameters (*S*-parameters) of the subarray for the three spacing cases are shown in Fig. 2. Note that, due to the symmetry of the subarray, it is sufficient to plot the reflection coefficients at ports 1-4 (corresponding to four elements in the left side of the subarray, see Fig. 1b). For the sake of clear exhibition, we only plot the mutual coupling coefficients between neighboring elements (i.e., the strongest mutual coupling). As expected, the mutual coupling increases as the inter-element spacing decreases. Due to the mutual coupling, the resonating frequency also increases as the inter-element spacing decreases. For fair comparison, we calculate the realized gain of RF beamforming (i.e., realized beamforming gain) and active reflection (i.e., the reflection coefficient at a port when all the ports are simultaneously excited) for each inter-element spacing case at a frequency where all the ports have reasonably high (> 20 dB) return losses, i.e., 28.3 GHz, 28.9 GHz and 31.1 GHz for $\lambda/2$, $\lambda/3$ and $\lambda/4$ inter-element spacing cases, respectively.

Figure 3 shows the realized beamforming gain at different scanning angles (where the broadside direction is 0°) for $\lambda/2$, $\lambda/3$ and $\lambda/4$ inter-element spacing cases. As can be seen the
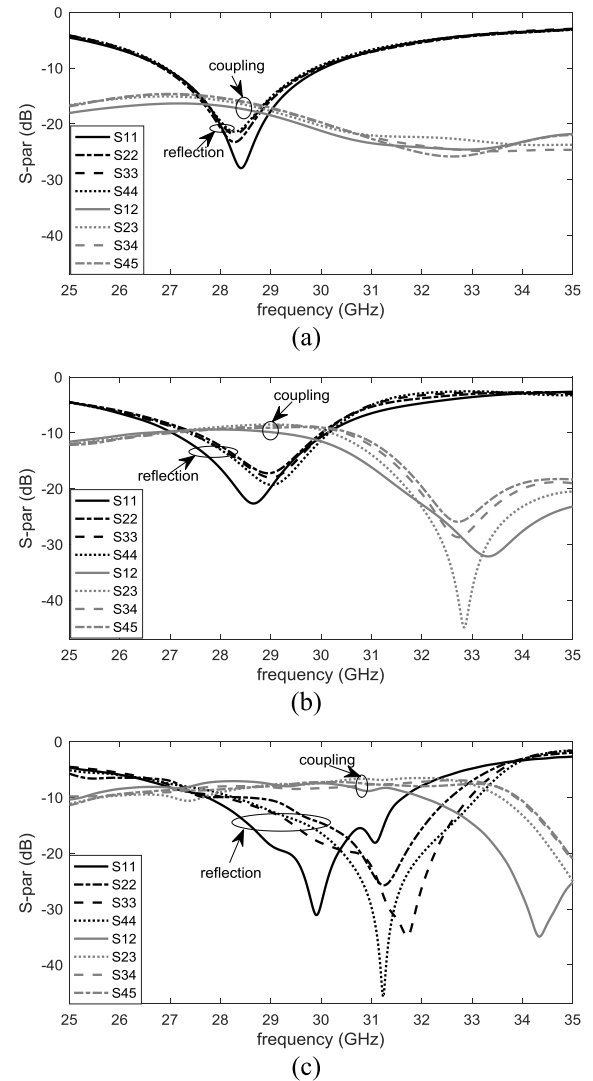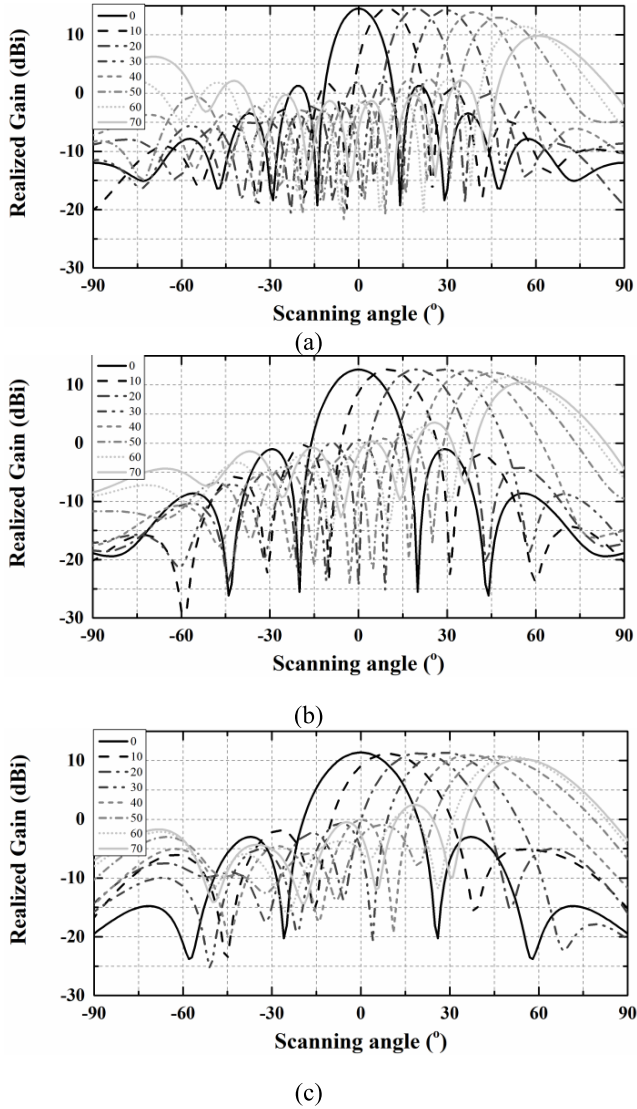

FIGURE 2. *S*-parameters of one subarray with (a) $\lambda/2$, (b) $\lambda/3$, and (c) $\lambda/4$ inter-element spacing.

realized beamforming gain and scanning (angle) range tend to decrease as we reduce the inter-element spacing (i.e., increase the mutual coupling). The reduction of the realized beamforming gain is due to smaller aperture of the array, and increased absorption loss and active reflection in the presence of mutual coupling (see Fig. 4), whereas the scanning range reduction is due to the decrease of inter-element spacing and the increase of mutual coupling. As can be seen from Fig. 3c, the realized gain becomes rather flat over the scanning range due to the increased mutual coupling [25]. However, this is achieved at the cost of an overall reduction of realized gain (i.e., a reduction of average power) and a reduced scanning range.
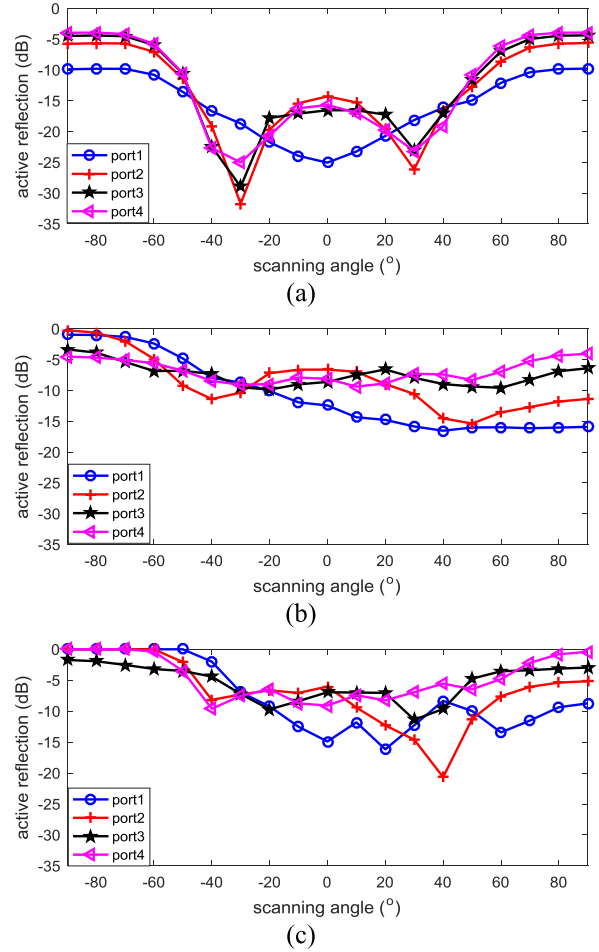
To demonstrate the mutual coupling effect on active reflections (or total active reflection coefficients), we plot the active reflections [26] at different ports of a subarray under different beam steering for the three inter-element spacing cases in Fig. 4. (The input reflection S_{ii} is calculated when only the *i*th port is excited while all the other ports are terminated with

FIGURE 3. Realized beamforming gain of one subarray with (a) $\lambda 2$, (b) $\lambda/3$, and (c) $\lambda/4$ inter-element spacing.

FIGURE 4. Active reflections at ports 1-4 of one subarray with (a) $\lambda/2$, (b) $\lambda/3$, and (c) $\lambda/4$ inter-element spacing under different scanning angles.

50-ohm loads, whereas the active reflection $\Gamma_i(\theta_0)$ is calculated when all the ports are excited to steer the beam to θ_0) It can be seen that the active reflection tends to grow as the mutual coupling increases and, more importantly, the active reflection increases with increasing scanning angle. One may notice that the active reflections at port 1 (i.e., the left most array element, cf. Fig. 1) are asymmetric with respect to the scanning angle for $\lambda/3$ and $\lambda/4$ spacing cases (e.g., its active reflection at $-90°$ scanning angle is larger than that at $90°$ scanning angle). This is because the left most element sees no elements when the array is beam steered toward the left endfire, whereas it sees all the other seven elements when the array is beam steered toward the right endfire. Due to this reason, the active refection at port 1 at a scanning angle β is the same with that at port 8 at scanning angle of $-\beta$, i.e., by flipping the active reflection (as a function of scanning angle) at port 1 from left to right, one get the active refection

at port 8. Hence, it suffices to show the active reflections of the left four elements (i.e., ports 1-4, see Fig. 1) only.

To show the mutual coupling effects on beam steering, we express the far field function of one beam steering subarray as [26]

$$g(\theta; \theta_0) = \frac{g_{\text{iso}}(\theta)}{\sqrt{N}} \sum_{n=1}^{N} (1 + \Gamma_n(\theta_0)) e^{j(n-1)kd(\sin(\theta) - \sin(\theta_0))} \quad (1)$$

where g_{iso} is the isolated far field function of one element, $N = 8$ is number of elements, θ_0 is the desired scanning angle (as can be seen from Fig. 3, at large scanning angle the main beam direction deviates from θ_0 in the presence of mutual coupling), $\Gamma_n(\theta_0) = \sum_{m=1}^{N} S_{nm} e^{j(m-n)kd\sin(\theta_0)}$ [26] is the active reflection at port n for scanning angle θ_0 (with Snm being the *S*-parameters), k is the wave number, and d is the inter-element spacing. As can be seen, the active reflection tends to increase as the mutual coupling increases, resulting in reduced realized beamforming gain and scanning range. Note that without loss of generality, we express the beam steering far field function only in xoz (theta) plane (see Fig. 1a) in (1), since the linear subarray cannot steer in the phi plane.

It is found from Figs. 3 and 4 that when setting the excitations to 70° scanning angle, the active reflections become so large that the actual angle of the steering beam becomes smaller than 70°. This is especially true for λ/3 and λ/4 spacing cases. Hence, it is safe to conclude that mutual coupling increases the active reflection and decreases the maximum scanning angle. Furthermore, the constraint on the maximum scanning angle implies an increase of outage probability in communications. (This is demonstrated by simulations in Section IV.)

III. MUTUAL COUPLING REDUCTION

The mutual coupling can be reduced by judicious design of the patch element. For fair comparison, we set the inter-element spacing to λ/2 thereafter.
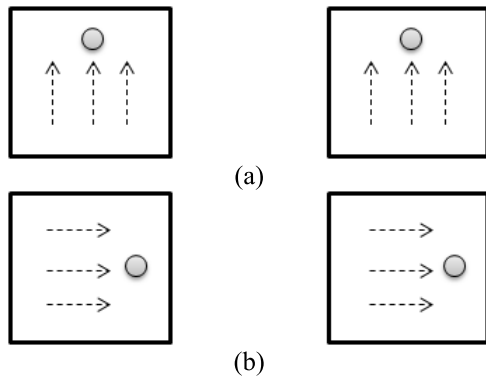

FIGURE 5. Drawing of a pair of square patches where the circles represent the feeding positions and dashed arrows denote the electrical currents: (a) broadside polarization; (b) endfire polarization.

The mutual coupling between patch elements mainly comes from two sources: radiation coupling and surface wave coupling. By making the polarizations of the element parallel (see Fig. 5a), the radiation coupling increases whereas the surface wave coupling decreases. Similarly, by making the polarizations of the elements collinear (see Fig. 5b), the radiation coupling decreases whereas the surface wave coupling increases. The dominance of the coupling source depends on the geometry of the patch element and the distance between the elements. The polarization of the patch element in the previous section is along the broadside of the linear subarray (i.e., broadside polarization), where the feeding position is about 0.85 mm (0.07λ) away from the center of the element. (Figure 5a shows an illustration of the feeding position and the polarization.) After rotating the patch element by 90°, the direction of the polarization becomes endfire (i.e., endfire polarization), as shown in Fig. 5b. It is found that for square patch elements with a (center-to-center) inter-element spacing of 0.5λ (edge-to-edge spacing of 0.25λ), the radiation coupling dominates, i.e., the endfire polarization case has lower mutual coupling. This is in agreement with the experimental finding in [27], where the broadside and endfire polarization cases are referred to as E-plane coupling and H-plane coupling, respectively.

The mutual coupling can be further improved by optimizing the orientation of the element and introducing notches in the ground plane. Figure 6 shows a new design of the handset array. It uses the same substrate, feeding cable and structure as that shown in Fig. 1. The patch elements are rotated by 45° along the z-axis, which reduce the mutual coupling to −24 dB. The dimension of the square patch is $L_P = 2.3$ mm. The feeding position is 0.7 mm from the patch center. Between every nearby patches, two notches of dimensions 2.3 mm × 0.2 mm (with a separation of 0.2 mm) are introduced in the ground plane (see Fig. 6b), which further reduce the mutual coupling to −32 dB. For simplicity, we refer to this array as the new design hereafter.
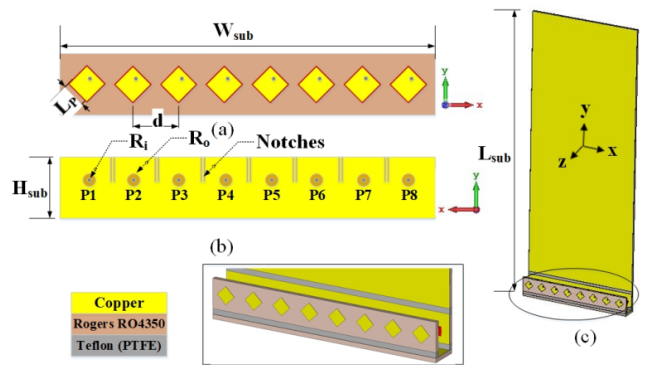

FIGURE 6. CST model of new design with improved mutual coupling: (a) front side of a subarray; (b) back side of a subarray; (c) the whole array composed of three subarrays together with chassis. The broadsides of the three subarrays are facing toward +z, −z, and −y directions, respectively. P1-P8 represents ports 1-8 of one subarray.
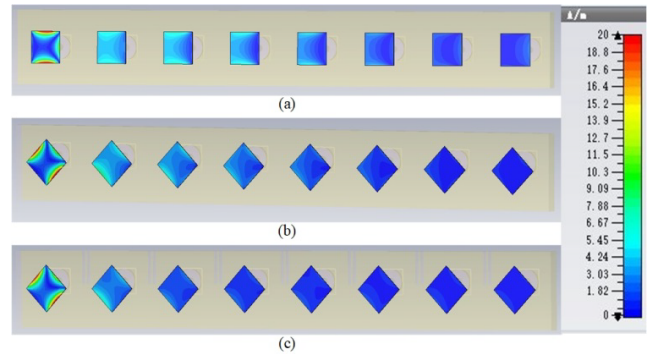
FIGURE 7. Surface current distributions: (a) Endfire polarization; (b) 45° rotation; (c) 45° rotation plus notches (new design). Port 1 is excited while the other ports are terminated with 50-ohm loads.

To show the decoupling effect, we plot surface current distribution of the subarrays with endfire polarization and the new designs with and without notches in Fig. 7. As can be seen, the mutual coupling reduces by rotating the array elements by 45°; and the isolation can be further enhanced by adding notches between the 45° tilted elements (at the cost of increased backward radiation though).

The corresponding *S*-parameters of the endfire polarization subarray and the new design are shown in Fig. 8. By comparing Fig. 2a and Fig. 8, one can see that the worst mutual
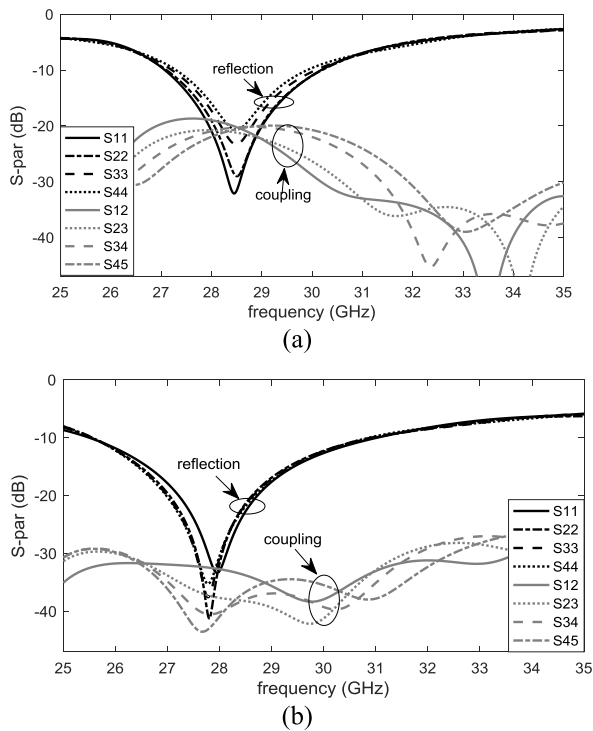
FIGURE 8. *S*-parameters of subarrays of (a) endfire polarization and (b) new design.
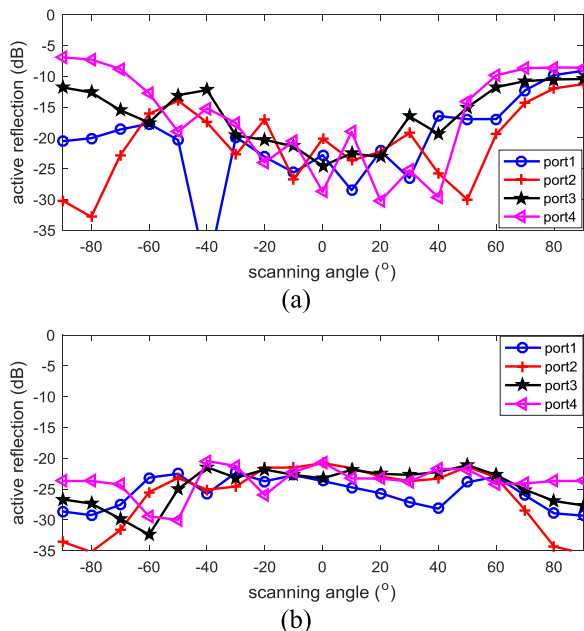

FIGURE 9. Active reflections at ports 1-4 of one subarray of (a) endfire polarization and (b) new design.

coupling (between neighboring elements) of the subarray with endfire polarization and the new design reduces by 4.7 dB and 16.7 dB, respectively, as compared with the original subarray with broadside polarization.

It can be seen by comparing Fig. 4a and Fig. 9 that, thanks to the mutual coupling reduction, the worst active reflections (among all the ports over the entire scanning ranges) of the
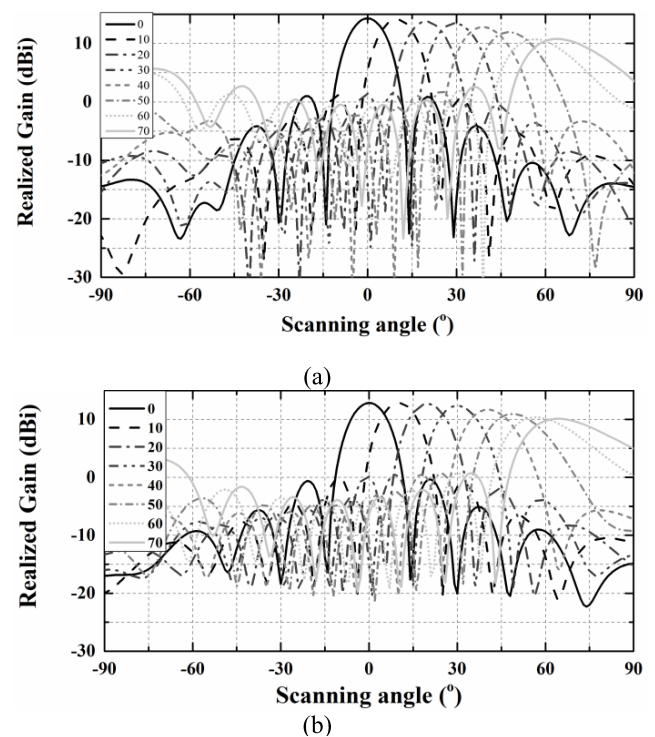
FIGURE 10. Realized beamforming gain of subarrays of (a) endfire polarization and (b) new design.

endfire polarization subarray and the new design are reduced by 6.9 dB to 20.4 dB, respectively, as compared with the original subarray with broadside polarization. Comparing Fig. 3a and Fig. 10, it can be seen that the scanning range also increases by about 5° and the realized beamforming gain increases by about 3 dB for both endfire polarization subarray and the new design, as compared with the original subarray with broadside polarization.

The reported worst mutual coupling of linear eight-element subarrays in [7], [12], and [13] are −17.0, −16.0, and −12.7 dB, respectively, whereas the worst mutual coupling of the endfire polarization subarray and the new design presented in this work are −19.0 and −32.0 dB, respectively. Despite the significant improvement of the mutual coupling, the realized beamforming gain of the new design is slightly lower than that of the endfire polarization subarray. This is because the notches introduced in the ground plane increases backward radiation and, therefore, reduce the element gain of the new design.

Note that, due to the random orientation of the user, the polarization of the mmWave handset array is also random. To reduce the probability of polarization mismatch between the base station and the user, ±45° tilted array elements are employed at the base station in practice [28]. This base station antenna configuration is assumed for simulations in the next section.

IV. SIMULATION
As mentioned in the introduction, mmWave handsets cannot afford to be fully digital. Thus, we cannot directly use the

MIMO capacity for performance evaluations of mmWave handset antennas. Instead, we need to consider initial access for the switch-based phased array antennas and use the effective beamforming channel for capacity evaluation. In this section, we evaluate the link-level performance of the (entire) handset array in terms of ergodic and outage capacities.

For simplicity, we assume the base station has acquired the information of the user location and performed hybrid beamforming towards the user. At the user side, we first sweep over the three subarrays and choose one that receives the highest power. Then we perform RF beamforming using the selected subarray. By using the bisection method (see Table 1) in searching for the strongest path, very fast initial access can be established at the user side. The initial access algorithm for the mmWave handset is summarized in Table 1.

TABLE 1. Initial access algorithm at the mmWave handset.

Let ϑ and $P(\vartheta)$ be the steering angle and the average received power at that angle.
1. Search for the subarray with the strongest average power
2. Search for the strong path using the selected subarray:
   1) Set initial searching angles:
$$\vartheta_L^{(0)} = -90° \quad \vartheta_R^{(0)} = 90° \quad \vartheta_M^{(0)} = 90° \,.$$
   2) If $P(\vartheta_M^{(i)}) > P(\vartheta_L^{(i)})$ & $P(\vartheta_M^{(i)}) > P(\vartheta_R^{(i)})$,
$$\vartheta_L^{(i+1)} = \left(\vartheta_L^{(i)} + \vartheta_M^{(i)}\right)/2$$
$$\vartheta_R^{(i+1)} = \left(\vartheta_R^{(i)} + \vartheta_M^{(i)}\right)/2$$
$$\vartheta_M^{(i+1)} = \vartheta_M^{(i)}$$
  else if $P(\vartheta_L^{(i)}) > P(\vartheta_M^{(i)})$,
$$\vartheta_L^{(i+1)} = \vartheta_L^{(i)}$$
$$\vartheta_R^{(i+1)} = \vartheta_M^{(i)}$$
$$\vartheta_M^{(i+1)} = \left(\vartheta_L^{(i+1)} + \vartheta_M^{(i+1)}\right)/2$$
  else
$$\vartheta_L^{(i+1)} = \vartheta_M^{(i)}$$
$$\vartheta_R^{(i+1)} = \vartheta_R^{(i)}$$
$$\vartheta_M^{(i+1)} = \left(\vartheta_R^{(i+1)} + \vartheta_M^{(i+1)}\right)/2$$
  end.
   3) Repeat step 2) until
$$\left|P(\vartheta_M^{(i+1)}) - P(\vartheta_M^{(i)})\right|/P(\vartheta_M^{(i)}) < 0.001 \text{ or } i \ge 10 \,.$$

In this work, we use the QuaDRiGa channel model [29] (i.e., a geometry-based stochastic channel model whose current version supports channel emulations up to 100 GHz). It is an extension of the well-known WINNER+ channel model [30]. Specifically in this work, we assume urban microcell scenario in line-of-sight condition at 28 GHz. The base station is located at the cellular center with a height of 10 m. The user is located randomly within one cellular sector at a height of 1.5 m. In order to focus on the antenna effect, we disable path loss in the channel model. For each realization (drop), a random user orientation is assigned. In total, 100000 channel drops are generated. At each user location and orientation, the effective beamforming channel is recorded (after the initial access). The same procedure is repeated for the switch-based phased array antennas with
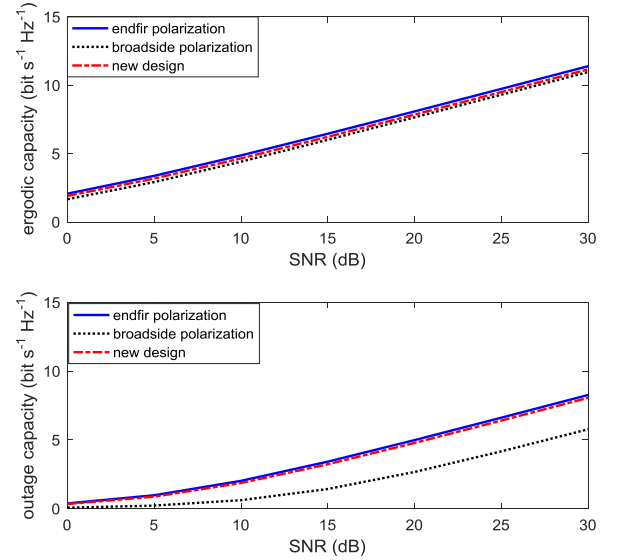
FIGURE 11. Comparisons of ergodic capacities and outage capacities (at 0.01 outage probability) of the three handset arrays.

endfire and broadside polarizations and the new design (see Figs. 5 and 6) at the user side. Both ergodic and outage capacities of the three array antennas are calculated using (2) and (3), respectively. The corresponding results are shown in Fig. 11.

$$C_{\text{ergodic}} = E\left[\log_2\left(1 + \gamma \, |h_{\text{eff}}|^2\right)\right] \quad (2)$$

$$C_{\text{outage}} = \log_2\left[1 + F^{-1}\left(1 - \varepsilon\right)\gamma\right] \quad (3)$$

where E denotes expectation, γ represents the reference signal-to-noise ratio (SNR), h_{eff} denotes the effective beamforming channel, F is the complementary cumulative distribution function of $|h_{\text{eff}}|^2$, and ε is the outage probability [24].

It can be seen from Fig. 11 that the switch-based phased array with endfire polarization outperforms that with broadside polarization. This is attributed to the reduced mutual coupling and increased scanning range. (Note that the mutual coupling between different subarrays is much lower than that within one subarray. Moreover, mutual coupling between different subarrays are less important in that, at any time instant, only one subarray can be chosen via the switch.) Although the mutual coupling reduction within each subarray only results in marginal improvement of the ergodic capacity, it clearly improves the outage capacity at 0.01 outage probability. The improvement of the ergodic capacity is due to the reduced absorption loss and active reflection (i.e., improved average power thanks to the mutual coupling reduction). Nevertheless, since the mutual coupling of the broadside polarization case is already low (about −15 dB), the improvement of the ergodic capacity is insignificant. The reason for bigger improvement of outage capacity than ergodic capacity is that the mutual coupling reduction improves the scanning range and, therefore, reduces the outage probability (i.e., the probability that $|h_{\text{eff}}|^2$ falls below certain value), which is vital for mmWave communications. However, it is noted

that further reduction of mutual coupling of the new design does not improve the capacity performance, as compared with the endfire polarization case. This is because that the mutual coupling reduction achieved by the new design is at the cost of (slightly) reduced realized beamforming gain due to increased backward radiation caused by the notches in the ground plane of the new design. Nevertheless, the new design also clearly outperforms the broadside polarization case in terms of outage capacity due to the increased scanning range.

V. CONCLUSION

In this paper, we investigated the mutual coupling effect on switch-based phased array antennas for 5G mmWave mobile applications. It is shown that the mutual coupling in a phased array antenna can cause severe active reflections at large scanning angle, which in turn reduces the realized beamforming gain and limits the maximum scanning angle of the phased array antenna. It is also shown that, for the considered square patches with $\lambda/2$ inter-element spacing, the mutual coupling between neighboring patch elements can be effectively reduced (as compared with the broadside polarization case) by orientating the polarization of each element to the endfire direction. By resorting to link-level simulations using the QuaDRiGa channel model, it is shown that, the outage capacity of the mmWave handset can be clearly improved (due to the improved scanning range) by reducing the worst mutual coupling from -15.3 dB to -20.0 dB via element rotations. The mutual coupling can be further reduced below -30 dB by rotating the elements and introducing notches in the ground plane. However, the notches in the ground plane decrease the realized beamforming gain, which sets back the capacity improvement due to the reduced mutual coupling.

REFERENCES

[1] T. S. Rappaport *et al.*, "Millimeter wave mobile communications for 5G cellular: It will work!" *IEEE Access*, vol. 1, pp. 335–349, May 2013.

[2] R. He, B. Ai, G. L. Stüber, G. Wang, and Z. Zhong, "Geometrical-based modeling for millimeter-wave MIMO mobile-to-mobile channels," *IEEE Trans. Veh. Technol.*, vol. 67, no. 4, pp. 2828–2863, Apr. 2018.

[3] S. Wu, C.-X. Wang, E.-H. M. Aggoune, M. M. Alwakeel, and X. You, "A general 3-D non-stationary 5G wireless channel model," *IEEE Trans. Commun.*, vol. 66, no. 7, pp. 3065–3078, Jul. 2018.

[4] K. Guan *et al.*, "On millimeter wave and THz mobile radio channel for smart rail mobility," *IEEE Trans. Veh. Technol.*, vol. 66, no. 7, pp. 5658–5674, Jul. 2017.

[5] A. Alkhateeb, O. El Ayach, G. Leus, and R. W. Heath, Jr., "Channel estimation and hybrid precoding for millimeter wave cellular systems," *IEEE J. Sel. Topics Signal Process.*, vol. 8, no. 5, pp. 831–846, Oct. 2014.

[6] W. Hong, K.-H. Baek, Y. Lee, Y. Kim, and S.-T. Ko, "Study and proto-typing of practically large-scale mmWave antenna systems for 5G cellular devices," *IEEE Commun. Mag.*, vol. 52, no. 9, pp. 63–69, Sep. 2014.

[7] B. Yu, K. Yang, C.-Y.-D. Sim, and G. Yang, "A novel 28 GHz beam steering array for 5G mobile device with metallic casing application," *IEEE Trans. Antennas Propag.*, vol. 66, no. 1, pp. 462–466, Jan. 2018.

[8] Y. J. Cheng and Y. Fan, "Millimeter-wave miniaturized substrate integrated multibeam antenna," *IEEE Trans. Antennas Propag.*, vol. 59, no. 12, pp. 4840–4844, Dec. 2011.

[9] Q.-L. Yang, Y.-L. Ban, K. Kang, C.-Y.-D. Sim, and G. Wu, "SIW multibeam array for 5G mobile devices," *IEEE Access*, vol. 4, pp. 2788–2796, 2016.

[10] B. Xu *et al.*, "Radiation performance analysis of 28 GHz antennas integrated in 5G mobile terminal housing," *IEEE Access*, vol. 6, pp. 48088–48101, 2018.

[11] W. Fan, P. Kyösti, M. Rumney, X. Chen and G. F. Pedersen, "Over-the-air radiated testing of millimeter-wave beam-steerable devices in a cost-effective measurement setup," *IEEE Commun. Mag.*, vol. 56, no. 7, pp. 64–71, Jul. 2018.

[12] S. Zhang, X. Chen, I. Syrytsin, and G. F. Pedersen, "A planar switchable 3-D-coverage phased array antenna and its user effects for 28-GHz mobile terminal applications," *IEEE Trans. Antennas Propag.*, vol. 65, no. 12, pp. 6413–6421, Dec. 2017.

[13] N. Ojaroudiparchin, M. Shen, S. Zhang, and G. F. Pedersen, "A switchable 3-D-coverage-phased array antenna package for 5G mobile terminals," *IEEE Antennas Wireless Propag. Lett.*, vol. 15, pp. 1747–1750, Feb. 2016.

[14] I. Syrytsin, S. Zhang, G. F. Pedersen, K. Zhao, T. Bolin, and Z. Ying, "Statistical investigation of the user effects on mobile terminal antennas for 5G applications," *IEEE Trans. Antennas Propag.*, vol. 65, no. 12, pp. 6596–6605, Dec. 2017.

[15] R. Khan, A. A. Al-Hadi, P. J. Soh, M. R. Kamarudin, M. T. Ali, and O. Owais, "User influence on mobile terminal antennas: A review of challenges and potential solution for 5G antennas," *IEEE Access*, vol. 6, pp. 77695–77715, 2018.

[16] K. Zhao *et al.*, "Spherical coverage characterization of 5G millimeter wave user equipment with 3GPP specifications," *IEEE Access*, vol. 7, pp. 4442–4452, 2019.

[17] X. Chen, S. Zhang, and Q. Li, "A review of mutual coupling in MIMO systems," *IEEE Access*, vol. 6, pp. 24706–24719, 2018.

[18] I. Nadeem and D.-Y. Choi, "Study on mutual coupling reduction technique for MIMO antennas," *IEEE Access*, vol. 7, pp. 563–586, 2019.

[19] L. Zhao, L. K. Yeung, and K.-L. Wu, "A coupled resonator decoupling network for two-element compact antenna arrays in mobile terminals," *IEEE Trans. Antennas Propag.*, vol. 62, no. 5, pp. 2767–2776, May 2014.

[20] A. Dadgarpour, B. Zarghooni, B. S. Virdee, T. A. Denidni, and A. A. Kishk, "Mutual coupling reduction in dielectric resonator antennas using metasurface shield for 60-GHz MIMO systems," *IEEE Antennas Wireless Propag. Lett.*, vol. 16, pp. 477–480, 2017.

[21] F. Liu, J. Guo, L. Zhao, X. Shen, and Y. Yin, "A meta-surface decoupling method for two linear polarized antenna array in sub-6 GHz base station applications," *IEEE Access*, vol. 7, pp. 2759–2768, 2019.

[22] H. Li, B. K. Lau, Z. Ying, and S. He, "Decoupling of multiple antennas in terminals with chassis excitation using polarization diversity, angle diversity and current control," *IEEE Trans. Antennas Propag.*, vol. 60, no. 12, pp. 5947–5957, Dec. 2012.

[23] K.-L. Wu, C. Wei, X. Mei, and Z.-Y. Zhang, "Array-antenna decoupling surface," *IEEE Trans. Antennas Propag.*, vol. 65, no. 12, pp. 6728–6738, Dec. 2017.

[24] A. Paulraj, R. Nabar, and D. Gore, *Introduction to Space-Time Wireless Communications*. Cambridge, U.K.: Cambridge Univ. Press, 2003.

[25] Y. Wang, L. Zhu, H. Wang, Y. Luo, and G. Yang, "A compact, scanning tightly coupled dipole array with parasitic strips for next-generation wireless applications," *IEEE Antennas Wireless Propag. Lett.*, vol. 17, no. 4, pp. 534–537, Apr. 2018.

[26] D. M. Pozar, "A relation between the active input impedance and the active element pattern of a phased array," *IEEE Trans. Antennas Propag.*, vol. 51, no. 9, pp. 2486–2489, Sep. 2003.

[27] R. P. Jedlicka, M. T. Poe, and K. R. Carver, "Measured mutual coupling between microstrip antennas," *IEEE Trans. Antennas Propag.*, vol. AP-29, no. 1, pp. 147–149, Jan. 1981.

[28] A. Alieldin, Y. Huang, M. Stanley, S. D. Joseph, and D. Lei, "A 5G MIMO antenna for broadcast and traffic communication topologies based on pseudo inverse synthesis," *IEEE Access*, vol. 6, pp. 65935–65944, 2018.

[29] S. Jaeckel, L. Raschkowski, K. Börner, and L. Thiele, "QuaDRiGa: A 3-D multi-cell channel model with time evolution for enabling virtual field trials," *IEEE Trans. Antennas Propag.*, vol. 62, no. 6, pp. 3242–3256, Jun. 2014.

[30] J. Meinilä *et al.*, "D5.3: WINNER+ final channel models," Tech. Rep., 2010.
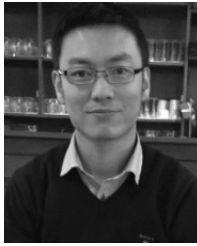
XIAOMING CHEN (M'16) received the B.Sc. degree in electrical engineering from Northwestern Polytechnical University, Xi'an, China, in 2006, and the M.Sc. and Ph.D. degrees in electrical engineering from the Chalmers University of Technology, Gothenburg, Sweden, in 2007 and 2012, respectively, where he was a Postdoctoral Researcher, from 2013 to 2014. From 2014 to 2017, he was with Qamcom Research and Technology AB, Gothenburg, Sweden. Since 2017, he has been a Professor with Xi'an Jiaotong University, Xi'an. His research areas include MIMO antennas, over-the-air testing, reverberation chambers, and hardware impairments and mitigation. He received the Outstanding Associate Editor (AE) Award, in 2018. He received the International Union of Radio Science Young Scientist Award, in 2017 and 2018. He serves as an AE for the IEEE Antennas and Wireless Propagation Letters.

MUHAMMAD ABDULLAH received the B.S. degree in telecommunication engineering from the University of Engineering and Technology, Peshawar, Pakistan, in 2016. He is currently pursuing the M.S. degree in information and communication engineering with Xi'an Jiaotong University, China. His research interest includes antenna design for different applications.
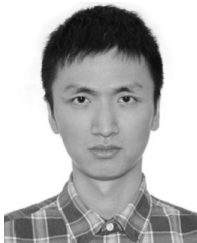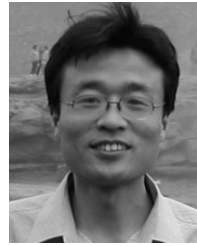
QINLONG LI received the B.S. degree from Xi'an Jiaotong University, Xi'an, China, in 2010, the M.S. degree from the University of Chinese Academy of Sciences, Beijing, China, in 2013, and the Ph.D. degree from the University of Hong Kong, Hong Kong, China. He is currently a Lecturer with Xi'an Jiaotong University. His research interests include antenna and metamaterial design.
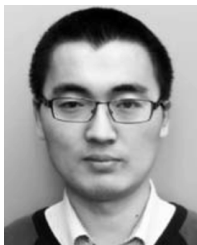
JIANXING LI (S'15–M'18) received the B.S., M.S., and Ph.D. degrees in electromagnetic field and microwave technology from Xi'an Jiaotong University, Xi'an, China, in 2008, 2011, and 2016, respectively. From 2014 to 2016, he was a Visiting Researcher with the Department of Electrical and Computer Engineering, Duke University, Durham, NC, USA, under the financial support from the China Scholarship Council. He is currently a Lecturer with the School of Electronic and Information Engineering, Xi'an Jiaotong University. His current research interests include antennas, microwave and mmWave circuits, and metamaterials. He serves as a Reviewer for several international journals, including the IEEE Access, the *IET Electronics Letters*, the *International Journal of RF and Microwave Computer-Aided Engineering*, and the *International Journal of Electronics and Communications*.

ANXUE ZHANG received the B.S. degree in electrical engineering from Henan Normal University, in 1996, and the M.S. and Ph.D. degrees in electromagnetic and microwave engineering from Xi'an Jiaotong University, in 1999 and 2003, respectively, where he is currently a Professor. His main research fields include antenna and electromagnetic wave propagation, RF and microwave circuit design, and metamaterials.

TOMMY SVENSSON (S'98–M'03–SM'10) received the Ph.D. degree in information theory from the Chalmers University of Technology, Gothenburg, Sweden, in 2003. He was with Ericsson AB, where he was involved in core networks, radio access networks, and microwave transmission products. He was involved in the European WINNER and ARTIST4G projects that made important contributions to the 3GPP LTE standards and the EU FP7 METIS and the EU H2020 5GPPP mmMAGIC 5G projects, and currently in the EU H2020 5GPPP 5GCar Project. He is currently with the ChaseOn Antenna Systems Excellence Center, Chalmers University of Technology, targeting mm-wave solutions for 5G access, backhaul, and V2X scenarios. He is also a Full Professor in communication systems with the Chalmers University of Technology, where he is leading the wireless systems research on air interface and wireless backhaul networking technologies for future wireless systems. He has co-authored four books, 77 journal papers, 121 conference papers, and 51 public EU projects deliverables. His research interests include the design and analysis of physical layer algorithms, multiple access, resource allocation, cooperative systems, moving networks, and satellite networks. He is the Chairman of the IEEE Sweden Joint Vehicular Technology/Communications/Information Theory Societies Chapter and an Editor of the IEEE Transactions on Wireless Communications. He has been an Editor of the IEEE Wireless Communications Letters and a Guest Editor of several top journals. He has organized several tutorials and workshops at top IEEE conferences and served as the Coordinator of the Communication Engineering Master's Program at the Chalmers University of Technology.

• • •